Atom cooling and trapping by disorder

Peter Horak, Jean-Yves Courtois, and Gilbert Grynberg

Laboratoire Kastler-Brossel, Département de Physique de l'Ecole Normale Supérieure, 24 rue Lhomond,

75231 Paris Cedex 05, France

We demonstrate the possibility of three-dimensional cooling of neutral atoms by illuminating them with *two* counterpropagating laser beams of mutually orthogonal linear polarization, where one of the lasers is a speckle field, i.e., a highly disordered but stationary coherent light field. This configuration gives rise to atom cooling in the *transverse* plane via a Sisyphus cooling mechanism similar to the one known in standard two-dimensional optical lattices formed by several plane laser waves. However, striking differences occur in the spatial diffusion coefficients as well as in local properties of the trapped atoms. [S1050-2947(98)06411-7]

PACS number(s): 32.80.Pj, 42.50.Vk

I. INTRODUCTION

The study of speckle laser patterns, as created when a highly coherent light beam is transmitted through or reflected from an object with a surface which is rough on the scale of the laser wavelength, was initiated many years ago using electromagnetic theory [1] and statistical methods [2,3]. Since then, this subject has raised more and more interest, resulting in a vast development of the theory (for a survey of the most recent results, see, e.g., Ref. [4]) as well as experimental achievements. These give rise to important applications of laser speckles in various fields of science, such as the speckle reduction in imagery [5], roughness measurements in material science [6], or applications in biophysics [7].

The scope of the work presented here is to investigate the application of such speckle laser fields in the context of laser cooling of neutral atoms. We are especially interested in the disordered analog of the so-called optical lattices formed by several laser plane waves, which yield periodic optical potentials and have been demonstrated experimentally to give rise to efficient laser cooling by a Sisyphus-type mechanism [8–10]. The basic principle of this cooling scheme is that the atoms lose kinetic energy by running up potential hills, from where they are optically pumped into lower-lying potential wells. Recent experiments have also demonstrated a similar cooling scheme in the case of laser configurations forming quasiperiodic optical lattices [11], which can be viewed as an intermediate regime between the standard periodic lattices and the completely disordered patterns obtained from speckle light fields.

We consider two counterpropagating laser fields of mutually orthogonal polarization, where one of the beams is a speckle field. According to the randomly distributed phase and intensity gradients of the speckle field in all dimensions, we find three-dimensional Sisyphus cooling even with this one-dimensional beam configuration. Moreover, interesting transport phenomena are found in this case, e.g., a large difference in the spatial diffusion of the atoms even in parameter regimes where the steady-state temperatures are of the same order of magnitude for the longitudinal and the transverse directions. Other effects, such as local radiation pressure forces, also arise from the fact that the amplitude and phase of the speckle field are essentially independent.

The paper is organized as follows. In Sec. II we qualitatively discuss our proposed setup and the basic physical processes which give rise to the cooling mechanism. In Sec. III we present the details of the theory and outline the numerical methods, especially the semiclassical Monte Carlo simulations, to obtain the results. Section IV is attributed to an analysis of the numerically obtained results such as temperatures, spatial diffusion coefficients, and local effects in the light field. Finally, in Sec. V we discuss the differences of the cooling in the laser propagation direction and in the transverse plane.

II. QUALITATIVE DISCUSSION

Throughout this paper we will discuss the simple situation of a single atom with a ground state of total angular momentum $F = \frac{1}{2}$ and an excited state with $F' = \frac{3}{2}$ interacting with two counterpropagating laser fields of orthogonal polarization. In the case of both laser fields being plane waves, this gives rise to well-known sub-Doppler cooling mechanisms in one dimension [12]. Because of the modulation of the optical potential, trapping of atoms in the longitudinal direction has been predicted [13] and observed [14]. In contrast, the atoms are free in the transverse plane.

In the situation discussed here, one of the laser fields is replaced by a speckle field, i.e., by a highly disordered, but nevertheless stationary and coherent light field. Such a speckle field can be easily generated experimentally, for instance, by introducing a diffusor into the path of a laser plane wave. The resulting light field shows highly disordered intensity and phase distributions (for a discussion of the statistical properties of speckle fields see, e.g., Ref. [2]). An example of a computer-generated speckle field on a discrete spatial grid is shown in Fig. 1.

Although different setups for the polarizations of the counterpropagating light fields give rise to cooling, we will concentrate here on the case of two mutually orthogonal linearly polarized fields (lin⊥lin configuration).

For this configuration one finds in the laser propagation direction, essentially the usual one-dimensional (1D) Sisyphus cooling mechanism [12] apart from the different spatial variation of intensity and phase of the speckle field as compared to a plane wave. Additionally, the properties of the
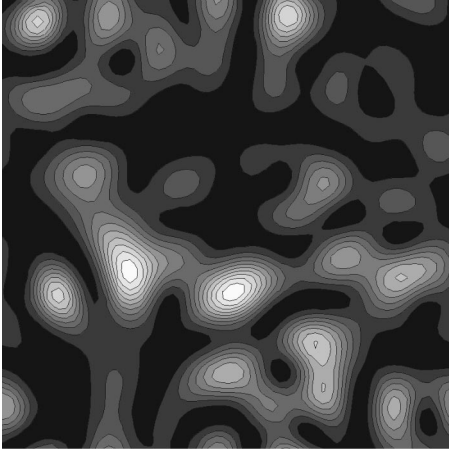
FIG. 1. Contour plot of the intensity of a numerically created speckle field on a grid of 64×64 points.

speckle field give rise to Sisyphus cooling of the atom in the transverse plane, since the phase and intensity modulations in these directions lead to spatially varying light shifts and optical pumping rates of the Zeeman sublevels of the atomic ground state. Thus the two counterpropagating laser beams (one plane wave and one speckle field) allow for *three-dimensional cooling* of the atom, in sharp contrast to the 1D lin⊥lin optical lattices used so far [15].

The most striking difference to the configuration of counterpropagating plane waves will be found in the transverse plane. Hence in the remainder of this paper we will mainly restrict ourselves to a 2D model of cooling in the transverse directions, and will only briefly discuss the changes induced by a model including the longitudinal direction in Sec. V.

As an example we plot the steady-state temperature reached in this 2D subsystem versus the optical potential depth $\hbar\Delta'$ for fixed optical pumping rate γ' in Fig. 2, where Δ' and γ' for the speckle field are defined with respect to the mean intensity of the beam. The numerical method to obtain these results will be described in detail in Sec. III. As our first and most important result we note that, as expected from the previous discussions, the atoms reach a steady-state temperature in the transverse plane. Second, the general behavior of this steady-state temperature as a function of the optical potential depth resembles very much the case of the standard optical lattices consisting of plane laser waves, i.e., for large values of Δ' one finds a linear dependence, and hence the
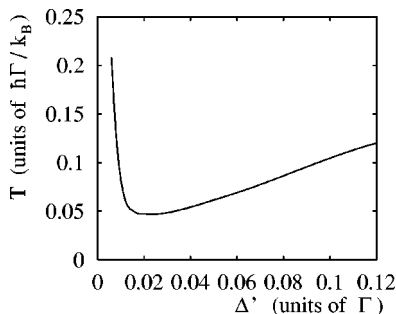

FIG. 2. Temperature T vs optical potential depth $\hbar\Delta'$ for a fixed optical pumping rate $\gamma' = 0.003\Gamma$, where Γ is the natural linewidth of the atomic excited state. The average speckle grain size is $d_{sp} = 3.8\lambda$.

steady-state kinetic energy becomes constant relative to the depth of the optical potentials in this limit. On the other hand, the temperature increases dramatically with small, decreasing values of Δ', and, finally, below a certain threshold value of Δ' no steady-state temperature is achieved. Consequently, one finds the lowest absolute values for the steady-state temperature for intermediate values of the optical potential depth.

According to this similarity with standard optical lattices, we may roughly estimate the steady-state temperature of the atoms in the speckle field from the formula

$$k_B T = \frac{\bar{D}}{\bar{\alpha}}, \tag{1}$$

where $\bar{D}$ is a mean momentum diffusion coefficient, and $\bar{\alpha}$ a mean friction coefficient [16]. Note that this formula only holds in the absence of atomic localization, which is not the case here, as we will see later, but nevertheless gives a useful order of magnitude for the temperature. The friction coefficient will be of the order of

$$\bar{\alpha} \sim \hbar k^2 \left(\frac{\lambda}{d_{sp}}\right)^2 \frac{\Delta}{\Gamma}, \tag{2}$$

where Δ is the detuning of the laser from the atomic resonance frequency, Γ is the natural linewidth of the excited state, and d_{sp} is the mean distance of neighboring intensity maxima along a 1D cut through the speckle field, i.e., the typical length scale of the speckle field. Equation (2) is obtained from the well-known expression for standard lattices [12,17,18], where we have only replaced the factors of λ by d_{sp}, which accounts for the different typical length scale.

The momentum diffusion coefficient can be guessed as

$$\bar{D} = \bar{D}_{dip} + \bar{D}_{se} \sim \hbar^2 k^2 \left(\frac{\lambda}{d_{sp}}\Delta'\right)^2 \frac{1}{\gamma'} + \gamma'\hbar^2 k^2, \tag{3}$$

which contains the diffusion $\bar{D}_{dip}$ due to the fluctuating dipole force and the diffusion $\bar{D}_{se}$ due to the recoil of the spontaneously emitted photons. $\bar{D}_{dip}$ is approximately given by the square of a typical force, $\hbar k (\lambda/d_{sp})(\Delta/\Gamma)$, times a typical time $1/\gamma'$, and $\bar{D}_{se}$ has the same form as for a standard lattice. Hence the estimated temperature (1) reads

$$\frac{k_B T}{\hbar\Delta'} \sim 1 + \left(\frac{d_{sp}}{\lambda}\right)^2 \left(\frac{\Gamma}{\Delta}\right)^2. \tag{4}$$

This formula exactly predicts the qualitative behavior of the temperature in Fig. 2, i.e., the linear increase for large values of Δ' and a rapid increase for very small values. It also shows that the lowest value of $T (= T_{min})$ is achieved for $\Delta'/\gamma' = d_{sp}/\lambda$, and that $k_B T_{min} = 2\hbar\gamma' d_{sp}/\lambda$. For a fixed optical pumping rate γ', the minimum temperature is thus expected to increase linearly with the speckle size.

III. THEORETICAL MODEL

In this section we give a more detailed discussion of the mathematical model and the numerical methods used to obtain the results presented in this paper.

A. Speckle fields

The first step for all the numerical treatments is to create a speckle field. This can be easily implemented on a computer following the procedure described in the work of Huntley [19], which we will briefly outline in the following.

Let us denote the electric field at the diffusor by $E_1(x,y)$ and the electric field at the plane chosen for the numerical simulations by $E_2(x,y)$. The two fields are related according to the Huygens-Fresnel principle in the Fresnel approximation by

$$E_2(x,y) = \frac{1}{\lambda l} \exp\left[-i\frac{\pi}{\lambda l}(x^2+y^2)\right] \int dx_1 dy_1 E_1(x_1,y_1)$$
$$\times \exp\left[-i\frac{\pi}{\lambda l}(x_1^2+y_1^2)\right] \exp\left[i\frac{2\pi}{\lambda l}(xx_1+yy_1)\right],$$
$$(5)$$

where l denotes the distance between the diffusor and the observation plane. Hence, if we define

$$E_1'(x,y) = E_1(x,y) \exp\left[-i\frac{\pi}{\lambda l}(x^2+y^2)\right], \qquad (6)$$

$$E_2'(x,y) = E_2(x,y) \exp\left[i\frac{\pi}{\lambda l}(x^2+y^2)\right], \qquad (7)$$

these two quantities are related by a Fourier transform.

Following [2] the real and imaginary part of $E_2'(x,y)$ at any point, (x,y) are independent Gaussian random variables. Thus the numerical construction of a speckle field starts by filling the real and imaginary parts of $E_2'(x,y)$ on a discrete spatial grid of $N\times N$ points with random numbers from a Gaussian distribution of zero mean and unit standard deviation. The grid size N must be chosen in such a way that it contains a reasonably large number of speckle grains, but nevertheless the discretized field must be smooth enough in order not to introduce large numerical errors. In practice we have used values of N between 64 and 256 for our calculations.

The effect of the finite size of the diffusor is implemented by transforming $E_2'(x,y)$ into $E_1'(x,y)$, multiplying the latter quantity by a window function $W(x,y)$ which assumes unity inside the diffusor and vanishes otherwise, and transforming the result back into a final $E_{2,\mathrm{fin}}'(x,y)$, i.e.,

$$E_{2,\mathrm{fin}}' = \mathcal{F}^{-1}(W\mathcal{F}(E_2')), \qquad (8)$$

where $\mathcal{F}$ denotes the two-dimensional Fourier transform.

B. Semiclassical model of atomic dynamics

As in most of the previous theoretical works on the Sisyphus cooling mechanism, including semiclassical [12,17,20] as well as quantum treatments [21,22], we consider the simple case of an atom with a ground state of angular momentum $F=\frac{1}{2}$ and an excited state of angular momentum $F'=\frac{3}{2}$. Furthermore we restrict ourselves to a 2D model and to the case of low atomic saturation, where we can adiabatically eliminate the excited state of the atom. The time evo-

lution of the atomic density operator restricted to the ground-state manifold is then governed by the master equation

$$\dot{\rho} = -\frac{i}{\hbar}[H,\rho] + L\rho, \qquad (9)$$

with the Hamiltonian

$$H = \hat{p}^2/2m + \hbar\Delta' V(\hat{x}) \qquad (10)$$

and the decay and recycling term

$$L\rho = (\gamma'/2)\left[-V(\hat{x})\rho - \rho V(\hat{x})\right.$$
$$\left. + 2\sum_\sigma \int d^2 q N(q) e^{-iq\hat{x}} B_\sigma^\dagger(\hat{x})\rho B_\sigma(\hat{x}) e^{iq\hat{x}}\right], \quad (11)$$

where the sum goes over the polarization and the integral over the wave vector of the spontaneously emitted photon projected into two dimensions. The optical potential depth is $\hbar\Delta'$, the optical pumping rate is γ', and the atomic transition operators $B_\sigma(\hat{x})$ and the optical potential operator $V(\hat{x})$ are defined as

$$B_\sigma(\hat{x}) = \left[\sum_\mu E_\mu(\hat{x})^\dagger A_\mu\right] A_\sigma^\dagger, \qquad (12)$$

$$A_\sigma = \sum_{m',m} \langle F',m'|1,\sigma;F,m\rangle |F',m'\rangle\langle F,m|, \qquad (13)$$

$$V(\hat{x}) = \sum_\sigma B_\sigma(\hat{x}) B_\sigma^\dagger(\hat{x}), \qquad (14)$$

where $E_\sigma(x)$ gives the spatial dependence of the σ-polarized laser light, and where we have made use of the Clebsch-Gordan coefficients in Eq. (13).

In order to derive a semiclassical theory suitable for Monte Carlo simulations we rewrite the master equation (9) in the Wigner representation defined by

$$W(x,p,t) = \frac{1}{(2\pi)^2} \int d^2 u \langle x+u/2|\rho(t)|x-u/2\rangle e^{-ipu}. \qquad (15)$$

Note that $W(x,p,t)$ is still an operator in the Hilbert space of the internal atomic degrees of freedom. However, for our specific choice of an atomic $F=\frac{1}{2}$ to $F'=\frac{3}{2}$ transition and the laser polarizations always lying within the same plane, no coherences between the ground-state sublevels build up. Hence the Wigner operator $W(x,p,t)$ remains diagonal,

$$W(x,p,t) = W_+(x,p,t)|m=\tfrac{1}{2}\rangle\langle m=\tfrac{1}{2}|$$
$$+ W_-(x,p,t)|m=-\tfrac{1}{2}\rangle\langle m=-\tfrac{1}{2}|. \qquad (16)$$

For these diagonal terms we obtain the Fokker-Planck equations

$$\dot{W}_\pm + \frac{p_i}{m}\partial_i W_\pm = -\gamma_{\pm\mp}W_\pm + \gamma_{\mp\pm}W_\mp + F^i_{\pm\pm}\partial_{p_i}W_\pm$$

$$+ F^i_{\mp\pm}\partial_{p_i}W_\mp + D^{ij}_{\pm\pm}\partial_{p_i}\partial_{p_j}W_\pm$$

$$+ D^{ij}_{\mp\pm}\partial_{p_i}\partial_{p_j}W_\mp, \tag{17}$$

where $i,j = x,y$, and a sum over i and j must be performed. The full expressions for the jump rates $\gamma_{\pm\mp}$ between the ground-state sublevels, the force coefficients $F^i_{\pm\pm}$, and the diffusion coefficients $D^{ij}_{\pm\pm}$ are given in the Appendix.

Finally, we use semiclassical Monte Carlo simulations [20] to obtain numerical solutions of Eqs. (17), where one follows the trajectories of many particles with internal states $|+\rangle$ and $|-\rangle$. The jump rates between these two states are given by γ_{+-} and γ_{-+}, respectively. Between two jumps the particles evolve according to the force F^i_{++} (F^i_{--}) acting on them, and in addition receive random kicks which are chosen in such a way as to simulate the effect of the diffusion terms D^{ij}_{++} (D^{ij}_{--}).

Averaging over a set of particles and over time yields all the required expectation values such as temperatures, mean local velocities, position distributions or spatial diffusion coefficients. We will discuss the most important results obtained in that way in Sec. IV.

C. Estimate of final temperature

Before turning to the numerical results obtained from solving the equations of motion presented in Sec. III B by Monte Carlo simulations, we will analytically derive a rough estimate for the steady-state temperature T obtained as the ratio of the mean momentum diffusion coefficient $\bar{D}$ over the mean friction coefficient $\bar{\alpha}$,

$$k_B T = \frac{\bar{D}}{\bar{\alpha}}, \tag{18}$$

where the bars over D and α denote averaging over the internal atomic state *and* over position. For simplicity we will restrict the following calculations only to the x direction.

In order to calculate the friction coefficient $\bar{\alpha}$ we must find the stationary solution $W(x,p)$ of Eq. (17) up to first order in the atomic velocity $v = p/m$, i.e., we expand $W(x,p)$ by

$$W(x,p) = W^0(x) + \frac{p}{m}W^1(x) + \cdots, \tag{19}$$

and insert this into Eq. (17). Since we are considering an atom moving with constant velocity, we may neglect the force and diffusion terms on the right-hand side of the equation, and thus obtain the results

$$W^0_+ = 1 - W^0_- = \frac{\gamma_{-+}}{\gamma_{-+} + \gamma_{+-}}, \tag{20}$$

$$W^1_+ = -W^1_- = -\frac{\partial_x W^0_+}{\gamma_{-+} + \gamma_{+-}}. \tag{21}$$

The friction coefficient, i.e., the term of first order in the velocity v of the force, averaged over the internal atomic state, is then given by

$$\alpha = F^x_{++}W^1_+ + F^x_{--}W^1_-. \tag{22}$$

Finally this must be averaged over the position within the speckle field. Since $F^x_{\pm\pm}$ as well as $W^1_\pm$ can be expressed in terms of the speckle electric-field amplitude and its spatial derivatives (see the Appendix), we need to know the expectation values of products of these quantities when averaged over position. Considering the complete randomness of the speckle field we assume that all averages over such products vanish except for

$$\overline{E_+ E^*_+} = \overline{E_- E^*_-} = 1, \tag{23}$$

assuming that the speckle field and the counterpropagating plane wave have the same average intensity, and

$$\overline{\partial_x E_+ \partial_x E^*_+} = \overline{\partial_x E_- \partial_x E^*_-}$$

$$= \frac{1}{2}k^2\left(\frac{\lambda}{d_{sp}}\right)^2 \overline{E_+ E^*_+}$$

$$= \frac{1}{2}k^2\left(\frac{\lambda}{d_{sp}}\right)^2, \tag{24}$$

where again d_{sp} is the mean speckle grain size. The right-hand side of Eq. (24) is obtained under the assumption that the required quantity for the speckle field is the same as for a periodic electric field with the same typical length scale, i.e., for an electric field given by $E(x) = \cos[kx(\lambda/d_{sp})]$. Applying these assumptions to Eq. (22) yields the friction coefficient

$$\bar{\alpha} = \hbar k^2 \frac{3\Delta}{4\Gamma}\left(\frac{\lambda}{d_{sp}}\right)^2. \tag{25}$$

The averaged diffusion coefficient has two different components. One of these is obtained by averaging the diffusion coefficients $D^{xx}_{\pm\pm}$ over the internal atomic states and over position similarly as done above for the friction coefficient. The second contribution to the total diffusion coefficient arises from the change of the dipole force, if the atom changes its internal state. This dipole diffusion term can be derived easily following the lines of Ref. [16]. We will omit all the calculational steps here and only give the final result for the total momentum diffusion coefficient

$$\frac{\bar{D}}{\hbar^2 k^2 \gamma'} = \frac{1}{2}\left(\frac{\Delta}{\Gamma}\right)^2\left(\frac{\lambda}{d_{sp}}\right)^2 + \frac{11}{36}\left(\frac{\lambda}{d_{sp}}\right)^2 + \frac{5}{36}, \tag{26}$$

where the first term is the dipole term and the second and third terms are due to the momentum diffusion of an atom in a definit internal state, i.e., coming from $D^{xx}_{\pm\pm}$.

Thus, for the estimated steady-state temperature (18), we obtain

$$\frac{k_B T}{\hbar \Delta'} = \frac{2}{3} + \frac{11}{27}\left(\frac{\Gamma}{\Delta}\right)^2 + \frac{5}{27}\left(\frac{\Gamma}{\Delta}\right)^2\left(\frac{d_{sp}}{\lambda}\right)^2. \tag{27}$$

We see that the expressions derived in Eqs. (25)–(27) are essentially the same as the intuitive ones of Sec. II.

It should be emphasized again that all quantities derived in this subsection should be considered as crude estimates, since they are performed in one dimension and rely on some
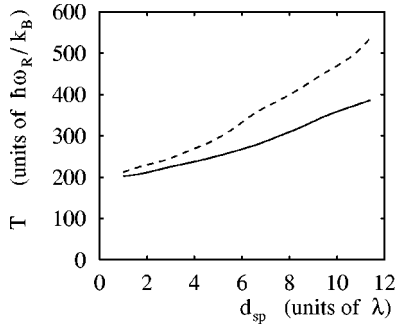
FIG. 3. Temperature vs speckle grain size for $\Delta'=200\omega_R$ and $\gamma'=13.33\omega_R$ (solid curve) and $20\omega_R$ (dashed curve), respectively.

FIG. 4. Temperature (2D) vs detuning Δ for fixed potential depth. Solid curve: $d_{sp}=1.9\lambda$ and $\Delta'=200\omega_R$; dashed curve: $d_{sp}=5.7\lambda$ and $\Delta'=200\omega_R$; dotted curve: $d_{sp}=1.9\lambda$ and $\Delta'=1000\omega_R$.

very rough approximations. However, the qualitative behavior of the exact solutions is predicted correctly, and thus these expressions provide a lot of physical insight.

Note further that the results derived here only hold in the regime of a friction force which is linear in the velocity, i.e., for velocities well below the capture range of the Sisyphus cooling. This capture range is characterized by a critical velocity v_c which corresponds to the velocity of an atom travelling from one optical potential well to the next one before being optically pumped [17], i.e.,

$$v_c = d_{sp}\gamma_{\pm\mp} = \tfrac{2}{9}d_{sp}\gamma'. \qquad (28)$$

Thus Eq. (27) is valid only for atomic kinetic energies below the critical value of $E_c = mv_c^2/2$ which depends linearly on the atomic mass. Therefore the critical energy is much lower for a light atom than for a heavy atom with the same optical properties.

On the other hand, the Monte Carlo simulations of Eq. (17) depend on the atomic mass, and give the correct velocity dependence of the force. Thus, in contrast to Eq. (27), the numerical simulations yield different steady-state temperatures for different atomic masses. Consequently, it is appropriate to introduce the mass as an additional sytem parameter, which is conveniently done in the form of the recoil frequency $\omega_R = \hbar k^2/(2m)$. In the following sections we will thus use ω_R as a fundamental unit (even if for a semiclassical theory the linewidth Γ seems better suited). All of our simulations were performed for cesium atoms, where $\Gamma \approx 2000\omega_R$, and where the mass is large enough that for most of the interesting parameter regimes the atomic velocity stays below v_c, and hence Eq. (27) can be applied.

IV. NUMERICAL RESULTS

A. Steady-state temperatures

As already shown in Sec. II, the general behavior of the steady-state temperature as a function of the optical potential depth is the same for our system as for optical lattices created by several plane waves. However, an important difference between the laser cooling inside a speckle field, as discussed here, and plane-wave lattices, lies in the tunability of the typical length scale. For our setup the mean speckle grain size d_{sp} can be changed continuously by changing the position of the diffusor which creates the speckle field out of a plane laser wave.
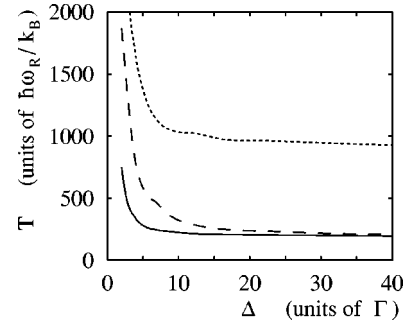
As an example, Fig. 3 shows the dependence of the

steady-state temperature on d_{sp}. As expected from the discussions in Sec. III, the temperature increases with larger speckle sizes. This feature arises from the fact that while the friction force decreases as $1/d_{sp}^2$ [cf. Eq. (25)], only the dipole term of the momentum diffusion [Eq. (26)] has the same dependence, whereas the sponaneous emission term remains constant. Hence the latter contribution of the total diffusion starts to dominate for large speckle sizes (more precisely for $d_{sp}/\lambda \gg \Delta'/\gamma'$), and hence the temperature is expected to increase quadratically with the speckle size.

The two curves of Fig. 3 correspond to the same optical potential depth Δ' but different optical pumping rates γ', i.e., different detunings Δ. In accordance with Eq. (27), the difference in temperature for small speckle grain size is small, but it becomes larger as soon as the term quadratic in d_{sp}/λ starts to dominate.

However, for the parameters chosen in Fig. 3, $\Delta'/\gamma' = 10$ (15), the temperature increases only by a factor of 3 (2), if the speckle grain size is increased from about λ to 12λ. But as we will discuss later in Sec. IV C, the increase of the spatial diffusion coefficient, which is equal to $\bar{D}/\bar{\alpha}^2$ in a certain range of parameters [18], is much larger.

In Fig. 4 we plot the steady-state temperature versus the detuning Δ for a fixed optical potential depth Δ', i.e., for a varying optical pumping rate γ'. The two lower curves correspond to the same optical potential depth but to a different speckle grain size d_{sp}. In agreement with Eq. (27) the temperature increases for smaller detunings Δ, i.e., larger pumping rates γ'. For very large detunings, corresponding to small values of γ', the temperature assumes a constant value, which is the same for different speckle sizes as long as the optical potential depth Δ' is the same. Hence in this limit the temperature becomes independent of the optical pumping rate γ' *and* of the speckle size d_{sp}. On the other hand, for a fixed speckle size but different values of Δ', the temperatures achieved in the limit of small values of γ' differ (cf. also Fig. 2).

B. Local properties

In this subsection we will discuss some of the localization properties of the cold atoms. To this end we give a contour plot of the steady-state atomic density ρ in Fig. 5(a), where the calculations have been performed for the speckle field depicted in Fig. 1. Comparing these two figures, one can see
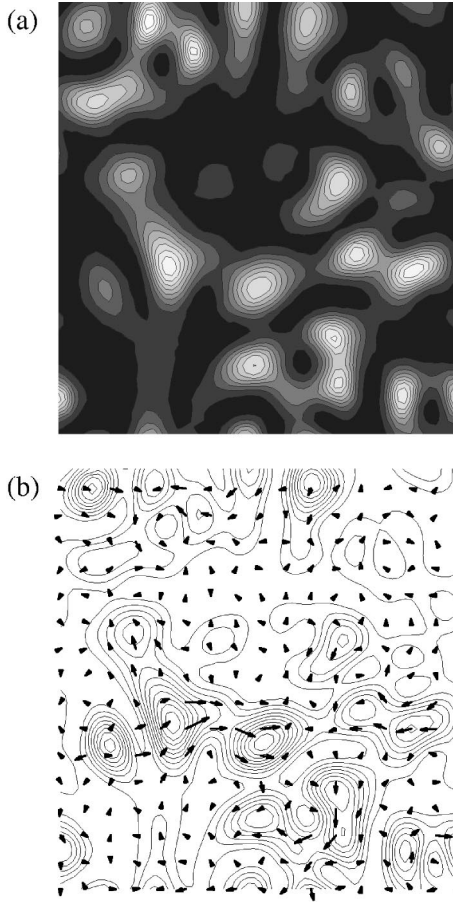
FIG. 5. (a) Contour plot of the atomic density for $\Delta' = 200\omega_R$ and $\gamma' = 13.33\omega_R$. (b) Contour plot of the speckle field intensity and vector field of the local radiation pressure force. The size of the spatial region is $(10\lambda)^2$.

easily that the atomic density is strongly correlated with the speckle field intensity I. This statistical dependence can be demonstrated more clearly by calculating the covariance, defined as

$$\text{cov}(\rho, I) = \langle \rho I \rangle / \sqrt{\langle \rho^2 \rangle \langle I^2 \rangle}. \tag{29}$$

We find that this quantity assumes values close to its maximum value of one, e.g., for Fig. 5(a), $\text{cov}(\rho, I) = 0.92$. This means that the intensity distribution of the speckle field is efficiently mapped onto the atomic density distribution.

However, if one looks closer at Figs. 1 and 5(a), one notes some discrepancies; for instance, some of the relatively shallow optical potential wells at the top of the figures are surprisingly strongly populated. Although these features cannot be explained quantitatively, we will describe some of the physical mechanisms in the following.

Basically these local differences are caused by the fact that the field amplitude and the phase of the speckle field are essentially uncorrelated. Whereas in usual optical lattices the light amplitude and phase are always correlated, which, e.g., in a 3D lin⊥lin setup yields that the optical potential minima coincide with places of pure circular polarization [8], this is not the case in our setup. Consequently the local polarization of the total light field at places of maximum local speckle field intensity can be linear as well as circular, but in general will be an arbitrary elliptical polarization. Hence only

speckle grains (regions of high speckle field intensity) of mainly circular polarization contribute to the Sisyphus-type cooling, but speckle grains of dominating linear polarization do not.

It should be emphasized that in speckle grains of mainly circular polarization *local cooling* can be found, that is, even within a single well an atom can be cooled by optical pumping processes between the widely differing optical potentials of the two ground-state sublevels. This is in contrast to the plane-wave 1D lin⊥lin configuration, where an atom must travel across several potential wells in order to be cooled (*nonlocal cooling*). Thus, the atom is more likely to be cooled and trapped within circularly polarized speckle grains.

Another reason for the different steady-state atomic densities in potential wells of the same depths is formed by the radiation pressure force. As already mentioned above, the light field amplitude and the phase of the speckle field are mutually independent, and thus the phase gradient can also differ strongly at the bottom of the potential wells. Hence, within some potential wells the atom experiences a relatively strong radiation pressure force and is thus pushed away. As an example, Fig. 5(b) again shows a contour plot of the speckle field intensity (the same as in Fig. 1), together with the vector field of the local radiation pressure force. This shows, e.g., a significant radiation pressure in the x direction in the high-intensity speckle grains at the center of the figure. Correspondingly, we have numerically found nonvanishing mean atomic velocities in these regions, which means that there exists a stationary flow of atoms following roughly the direction of the local radiation pressure force. This might suggest that a description of speckled lattices in terms of fluid mechanics formalism may be interesting to investigate; however, this is beyond the scope of this paper.

Finally we will briefly discuss the atomic density distribution $P(\rho)$, i.e., the probability of finding a certain density. A histogram plot for the speckle field intensity $P(I)$ and the atomic density is given in Fig. 6.

The numerically obtained speckle field intensity distribution, Fig. 6(a), follows an exponential law, as theoretically discussed in [2], with equal mean and standard deviation, i.e.,

$$P(I/\langle I \rangle) = \exp(-I/\langle I \rangle). \tag{30}$$

As can be seen from Fig. 6(b) the atomic density does not follow the same law, since there is always a background of unbound atoms, and hence the probability of finding a density below a certain threshold vanishes. But above this threshold the density distribution function closely resembles the speckle intensity distribution, which again indicates a strong correlation between the light field intensity and the atomic density.

C. Spatial diffusion

Another important quantity for characterizing the properties of the cooled and trapped atoms is the spatial diffusion coefficient, which roughly quantifies the transfer of atoms between several potential wells and hence of the spreading of an initially small atomic cloud. Experimentally, as well as in our Monte Carlo simulations, the spatial diffusion coefficient
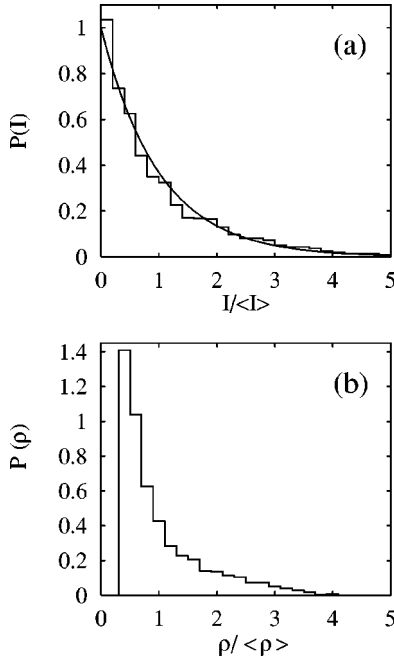
FIG. 6. (a) Histogram plot of a numerically obtained speckle field intensity. Theoretical analyses predict an exponential behavior (smooth curve). (b) Histogram plot of the atomic density for $\Delta' = 200\omega_R$, $\gamma' = 13.33\omega_R$, and $d_{sp} = 1.9\lambda$.

D_s is obtained from the spreading of an initial atomic cloud whose variance follows a linear law in the long-time limit,

$$[\Delta r(t)]^2 = [\Delta r(0)]^2 + 2D_s t. \tag{31}$$

An estimate for the value of D_s can be derived [18] by using

$$D_s = \frac{\bar{D}}{\bar{\alpha}^2} \tag{32}$$

for the spatial diffusion coefficient for a Brownian motion [23]. Applying our findings for the friction coefficient (25) and the momentum diffusion (26), we obtain

$$D_s = \frac{8}{9} \frac{\gamma'}{k^2} \left(\frac{d_{sp}}{\lambda}\right)^2$$

$$\times \left[1 + \frac{11}{18}\left(\frac{\Gamma}{\Delta}\right)^2 + \frac{5}{18}\left(\frac{\Gamma}{\Delta}\right)^2\left(\frac{d_{sp}}{\lambda}\right)^2\right]. \tag{33}$$

We can now compare this with the spatial diffusion coefficients obtained by semiclassical Monte Carlo simulations, as depicted in Fig. 7 as a function of the detuning Δ. It follows from Eq. (33) that for $\gamma'/\Delta' = \Gamma/\Delta \ll 1$ the first term will dominate, and hence the spatial diffusion coefficient scales linearly with γ', i.e., like $1/\Delta$ if Δ' is kept constant. This is in qualitative agreement with the curves of Fig. 7 for not too large values of the detuning Δ. However, Eq. (33) only holds if the atom moves only a fraction of the speckle size d between two optical pumping processes [18], which explains the deviation of the numerically obtained curves from the $1/\Delta$ law for large values of Δ.

Note that for $\Delta \gg \Gamma$, and within its range of validity, Eq. (33) predicts an increase of the spatial diffusion coefficient with the square of the speckle grain size. This has been nicely confirmed by our numerical simulations. For an actual
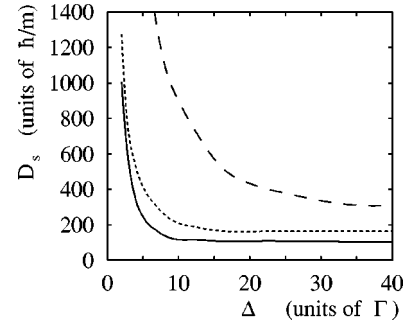

FIG. 7. Spatial diffusion vs detuning Δ for fixed potential depth. Solid curve: $d_{sp} = 1.9\lambda$ and $\Delta' = 200\omega_R$; dotted curve: $d_{sp} = 1.9\lambda$ and $\Delta' = 1000\omega_R$; dashed curve: $d_{sp} = 5.7\lambda$ and $\Delta' = 200\omega_R$. (For the corresponding steady-state temperatures, see Fig. 4.)

experiment, where the speckle size is typically of the order of tens of wavelengths, this means that the spatial diffusion of the atoms in the speckle field can easily be orders of magnitude larger than for a standard optical lattice, even if the steady-state temperatures (27) are comparable.

V. INFLUENCE OF THE LONGITUDINAL DIRECTION

Compared to the transverse directions, which have been discussed so far, the physical properties of the system along the laser propagation direction are completely different. First, it should be emphasized again that the size of the speckle grains in this direction is generally much larger, i.e., by a factor on the order of d_{sp}/λ. But superimposed on this relatively large length scale there is a standard 1D lin⊥lin configuration with a typical length scale of half an optical wavelength, such that the system must be characterized in this direction by two widely different length scales. Second, this superimposed lin⊥lin configuration leads to efficient cooling in the longitudinal direction at regions in space where the speckle field intensity approximately equals the intensity of the counterpropagating plane wave. However, at locations where the two beam intensities differ, it also leads to a nonbalanced radiation pressure force driving the atoms away from these locations. Note that the situation is similar to what can be found in quasiperiodic lattices [11].

Hence, the full 3D situation is much more intricate than the transverse 2D scheme. Also, numerically, a complete 3D treatment would be very demanding. Instead we performed some 2D simulations of the cooling dynamics including the longitudinal and one transverse direction, which should give some relevant information about the actual behavior of the system in three dimensions.

In Fig. 8 we depict the temperatures in the longitudinal direction and in the transverse direction obtained from such 2D Monte Carlo simulations. We see that the transverse temperatures are always higher than the longitudinal ones. Even if there exists a strong radiation pressure in the longitudinal direction in regions of differing speckle and plane wave intensity, this effect is overcompensated for by the much more efficient Sisyphus cooling in this direction.

Second, let us remark that the transverse temperatures are larger for this type of Monte Carlo simulations than those obtained from simulations including two transverse directions. Hence the inclusion of the longitudinal direction tends to reduce the efficiency of the transverse cooling. This can be
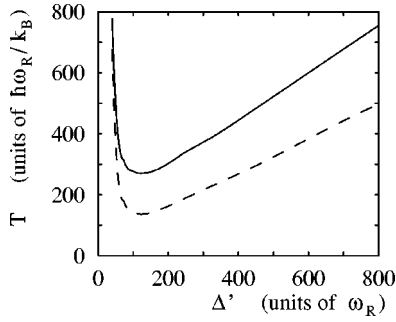
FIG. 8. Steady-state temperatures in the transverse direction (solid line) and in the longitudinal direction (dashed) for fixed optical pumping rate $\gamma' = 20\omega_R$ vs optical potential depth. The speckle grain size is $d_{sp} = 1.8\lambda$ transversally, and $d'_{sp} = 7.2\lambda$ longitudinally.

understood by the following arguments. Since the transverse cooling relies on a Sisyphus effect, it is more efficient for deeper potential wells because in this case a single quantum jump between the two adiabatic potentials reduces the atomic energy by a larger amount. Thus the cooling mechanism is most effective in regions of maximum speckle field intensity. But in the longitudinal direction, these regions correspond exactly to the regions of maximum radiation pressure, and hence the atom is efficiently pushed away. For the transverse cooling this means that the atom avoids the deepest potential wells, which consequently reduces the cooling efficiency and therefore increases the steady-state temperature.

For the spatial diffusion coefficient we found a much larger difference between the longitudinal and transverse directions than for the temperature. This agrees well with our previous results that the leading term in the expression of the temperature [Eq. (27)] is independent of the speckle size, whereas the spatial diffusion (33) scales with the square of the speckle size. Hence the difference in the typical length scale between the longitudinal direction (λ) and the transverse direction (d_{sp}) yields widely different spatial diffusion. Again we note that the values for the transverse spatial diffusion obtained by the Monte Carlo simulations with the longitudinal and one transverse direction lies above the value obtained from simulations restricted to the transverse plane, according to the reduced cooling efficiency as discussed above.

VI. CONCLUSIONS

In this work we have demonstrated that 3D laser cooling of neutral atoms can be achieved by a 1D setup, if one of the two counterpropagating laser beams of a plane-wave 1D optical ''molasses'' [14] is replaced by a speckle laser field [24]. The cooling mechanism in this case relies on a Sisyphus effect similar to the one known in usual (periodic) lattices [12] in one, two, and three dimensions. We have calculated steady-state temperatures similar to those obtained for periodic lattices for large red detunings of the lasers from the atomic resonance. In this far-detuned limit the steady-state temperatures also become independent of the mean speckle grain size.

In contrast to usual lattices we have found various local effects, such as local cooling and nonvanishing radiation

pressure forces which are essentially decoupled from the local optical potential depth. Furthermore, according to the speckle field the spatial diffusion of the atoms is increased by a factor of approximately the square of the typical speckle grain size.

Thus for an experimental realization of this scheme two points should be emphasized. First, the experimental setup is relatively simple since a 1D configuration is already sufficient to yield 3D sub-Doppler cooling. On the other hand, the obtained speckle grain size is typically much larger than an optical wavelength, which gives rise to longer cooling times and a huge increase of the spatial diffusion. Thus the lifetime of the trapped atomic cloud will be much shorter than in usual lattices, and the achievable atomic densities much lower. However, first experimental results [25] have already confirmed most of the theoretical predictions presented in this work, and reasonable agreement with the numerically obtained values for, e.g., the steady-state temperatures has been found.

Although such investigations and possible extensions of the scheme, e.g., to the study of speckled dark lattices, already present interesting results for laser cooling, we think that the main interest lies in the possibility of creating a disordered sample of cold atoms with well-controlled statistical characteristics. Because of the growing interest in the study of disordered materials, the presented system may thus be useful in this domain.

APPENDIX: FOKKER-PLANCK EQUATION

In the following we give exact expressions for the coefficients which appear in the Fokker-Planck equation (17) as obtained from the Wigner transform of the master equation (9) (the derivation is straightforward but lengthy and will thus be omitted). The jump rates read

$$\gamma_{\pm\mp} = \tfrac{2}{9}\gamma' |E_\mp|^2, \qquad (A1)$$

the force coefficients are

$$F^i_{\pm\pm} = \Delta' \left\{ (\partial_i E_\pm) E^\dagger_\pm + \frac{1}{3}(\partial_i E_\mp) E^\dagger_\mp + \text{c.c.} \right\}$$
$$+ \gamma' \frac{i}{2} \left\{ (\partial_i E_\pm) E^\dagger_\pm + \frac{1}{9}(\partial_i E_\mp) E^\dagger_\mp - \text{c.c.} \right\},$$
$$(A2)$$

$$F^i_{\mp\pm} = \gamma' \frac{i}{9} \{ (\partial_i E_\pm) E^\dagger_\pm - \text{c.c.} \}, \qquad (A3)$$

where $i = x, y$, and the diffusion coefficients are

$$D^{xx}_{\pm\pm} = \gamma' \frac{1}{8} \left\{ 4(\partial_x E_\pm)(\partial_x E^\dagger_\pm) + \frac{2}{9}(\partial_x \partial_x E_\mp) E^\dagger_\mp \right.$$
$$\left. + \frac{2}{9} E_\mp (\partial_x \partial_x E^\dagger_\mp) + \frac{8}{9}(\partial_x E_\mp)(\partial_x E^\dagger_\mp) \right\}$$
$$+ \gamma' \frac{k^2}{8} \left| E_\pm + \frac{1}{3} E_\mp \right|^2, \qquad (A4)$$

$$D_{\pm\pm}^{yy} = \gamma' \frac{1}{8}\left\{4(\partial_y E_\pm)(\partial_y E_\pm^\dagger) + \frac{2}{9}(\partial_y \partial_y E_\mp)E_\mp^\dagger\right.$$

$$\left. + \frac{2}{9}E_\mp(\partial_y \partial_y E_\mp^\dagger) + \frac{8}{9}(\partial_y E_\mp)(\partial_y E_\mp^\dagger)\right\}$$

$$+ \gamma' \frac{k^2}{8}\left|E_\pm - \frac{1}{3}E_\mp\right|^2, \tag{A5}$$

$$D_{\pm\pm}^{xy} = D_{\pm\pm}^{yx} = \gamma' \frac{1}{8}\left\{2(\partial_x E_\pm)(\partial_y E_\pm^\dagger) + \frac{2}{9}(\partial_x \partial_y E_\mp)E_\mp^\dagger\right.$$

$$\left. + \frac{4}{9}(\partial_x E_\mp)(\partial_y E_\mp^\dagger) + \text{c.c.}\right\}, \tag{A6}$$

$$D_{\mp\pm}^{ii} = -\gamma' \frac{1}{36}\{(\partial_i \partial_i E_\pm)E_\pm^\dagger + E_\pm(\partial_i \partial_i E_\pm^\dagger)$$

$$- 2(\partial_i E_\pm)(\partial_i E_\pm^\dagger)\} + \gamma' \frac{k^2}{18}|E_\pm|^2, \tag{A7}$$

$$D_{\mp\pm}^{xy} = D_{\mp\pm}^{yx} = -\gamma' \frac{1}{36}\{(\partial_x \partial_y E_\pm)E_\pm^\dagger$$

$$+ (\partial_x E_\pm)(\partial_y E_\pm^\dagger) + \text{c.c.}\}. \tag{A8}$$

For the derivation of the diffusion coefficients, we have simplified the spontaneous emission pattern by assuming that fluorescence photons are only emitted along the x, y, and z axes [20].

Two other points are worth a comment here concerning the application of these diffusion constants and forces in the semiclassical Monte Carlo simulations outlined in Sec. III B. First, it turns out that for all realistic choices of the system parameters the cross terms $F_{\mp\pm}^i$ and $D_{\mp\pm}^{ij}$ between the two ground-state sublevels can be neglected as compared with the terms $F_{\pm\pm}^i$ and $D_{\pm\pm}^{ij}$. Second, at some positions in space the diffusion coefficients assume negative values. This property indicates a purely quantum feature of the system, i.e., it shows that there exist positions in space where the atomic wavefunction collapses rather than spreads out [26]. However, this feature *cannot* be mimicked by the semiclassical simulations, where negative diffusion makes no sense. Hence, whenever this situation occurs in our numerical simulations we set the diffusion coefficients equal to zero to avoid this problem.

[1] P. Beckmann and A. Spizzichino, *The Scattering of Electromagnetic Waves from Rough Surfaces* (Pergamon, Oxford, 1963); P. Beckmann, in *Progress in Optics VI*, edited by E. Wolf (North-Holland, Amsterdam, 1967), pp. 55–69.

[2] J. W. Goodman, in *Laser Speckle and Related Phenomena*, edited by J. C. Dainty (Springer-Verlag, Berlin, 1975), pp. 9–75.

[3] J. C. Dainty, in *Progress in Optics XIV*, edited by E. Wolf (North-Holland, Amsterdam, 1977), pp. 1–46.

[4] Waves Random Media **7**, 283 (1997), special issue on wave scattering from rough surfaces and related phenomena, edited by A. A. Maradudin and M. Nieto-Vesperinas; **8**, 1 (1998).

[5] E. R. Harvey and G. V. April, Opt. Lett. **15**, 740 (1990).

[6] U. Persson, Opt. Eng. (Bellingham) **32**, 3327 (1993).

[7] Y. Aizu and T. Asakura, Opt. Laser Technol. **23**, 205 (1991).

[8] G. Grynberg and C. Triché, in *Coherent and Collective Interactions of Particles and Radiation Beams*, Proceedings of the International School of Physics ''Enrico Fermi,'' Course CXXXI, Varenna, 1995, edited by A. Aspect, W. Barletta, and R. Bonifacio (ETS Editrice, Pisa, 1996), p. 243.

[9] A. Hemmerich, M. Weidemüller, and T. W. Hänsch, in *Coherent and Collective Interactions of Particles and Radiation Beams* (Ref. [8]), p. 503.

[10] P. S. Jessen and I. H. Deutsch, Adv. At., Mol., Opt. Phys. **37**, 95 (1996).

[11] L. Guidoni, C. Triché, P. Verkerk, and G. Grynberg, Phys. Rev. Lett. **79**, 3363 (1997).

[12] J. Dalibard and C. Cohen-Tannoudji, J. Opt. Soc. Am. B **6**, 2023 (1989).

[13] Y. Castin and J. Dalibard, Europhys. Lett. **14**, 761 (1991).

[14] P. Verkerk, B. Lounis, C. Salomon, C. Cohen-Tannoudji, J.-Y. Courtois, and G. Grynberg, Phys. Rev. Lett. **68**, 3861 (1992); P. S. Jessen, C. Gerz, P. D. Lett, W. D. Phillips, S. L. Rolston, R. J. C. Spreeuw, and C. I. Westbrook, *ibid.* **69**, 49 (1992).

[15] In the different context of magneto-optical traps other schemes to achieve 3D cooling and trapping by only two laser beams have been suggested and experimentally demonstrated; see, e.g., C. Chesman *et al.*, Opt. Lett. **19**, 1237 (1994).

[16] J. Dalibard and C. Cohen-Tannoudji, J. Opt. Soc. Am. B **2**, 1707 (1985).

[17] C. Cohen-Tannoudji, in *Fundamental Systems in Quantum Optics*, Proceedings of the Les Houches Summer School, Session LIII, edited by J. Dalibard, J.-M. Raimond, and J. Zinn-Justin (North-Holland, Amsterdam, 1992), pp. 1–164.

[18] T. W. Hodapp, C. Gerz, C. Furthlehner, C. I. Westbrook, W. D. Phillips, and J. Dalibard, Appl. Phys. B: Photophys. Laser Chem. **60**, 135 (1995).

[19] J. M. Huntley, Appl. Opt. **28**, 4316 (1989).

[20] Y. Castin, K. Berg-Sørensen, J. Dalibard, and K. Mølmer, Phys. Rev. A **50**, 5092 (1994).

[21] P. Marte, R. Dum, R. Taïeb, and P. Zoller, Phys. Rev. A **47**, 1378 (1993).

[22] S. Marksteiner, K. Ellinger, and P. Zoller, Phys. Rev. A **53**, 3409 (1996).

[23] Note that this approximation is justified only in the regime of a friction force linear in velocity, i.e., well below the capture range of the Sisyphus cooling [Eq. (28)]. For very light atoms, where the capture range is rather small, the cooling of hot atoms is much less efficient, and thus the spatial diffusion can be much larger than the value given by Eq. (32).

[24] Although we focused this paper on the case of the lin⊥lin configuration, we also made some calculations for the

$\sigma_+ - \sigma_-$ case. In that situation a Sisyphus cooling occurs in the transverse plane because of the phase and intensity variations of the speckle field. However, the temperature is generally higher than the one found in the lin⊥lin configuration.

[25] C. Mennerat-Robilliard, D. Boiron, L. Guidoni, J. M. Fournier, P. Horak, and G. Grynberg, Europhys. Lett. (to be published).

[26] K. Berg-Sørensen, Y. Castin, E. Bonderup, and K. Mølmer, J. Phys. B **25**, 4195 (1992).